JAAS

Exploring the boundaries in the analysis of large particles by single particle inductively coupled plasma mass spectrometry: Application to nanoclays

Journal:	*Journal of Analytical Atomic Spectrometry*
Manuscript ID	JA-ART-01-2022-000026.R1
Article Type:	Paper
Date Submitted by the Author:	n/a
Complete List of Authors:	Ojeda, David; University of Zaragoza, a. Group of Analytical Spectroscopy and Sensors (GEAS), Institute of Environmental Sciences (IUCA) Bolea, Eduardo; Universidad de Zaragoza, Group of Analytical Spectroscopy and Sensors (GEAS), Institute of Environmental Sciences (IUCA) Perez-Arantegui, Josefina; University of Zaragoza, Department of Analytical Chemistry, IUCA Laborda, Francisco; University of Zaragoza, Group of Analytical Spectroscopy and Sensors (GEAS), Institute of Environmental Sciences (IUCA)

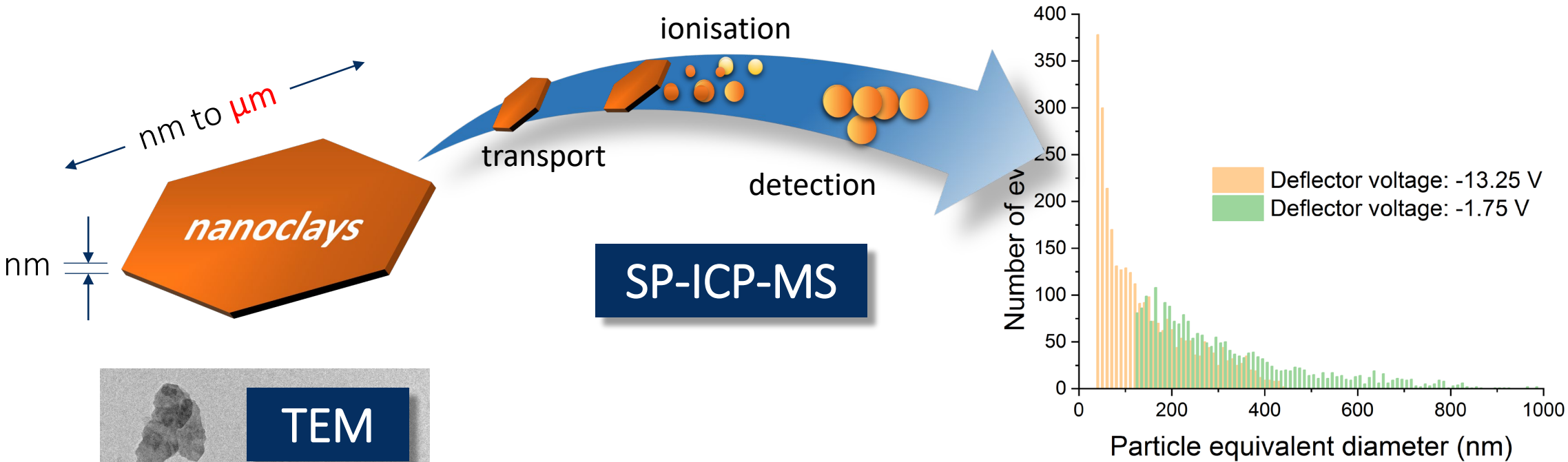

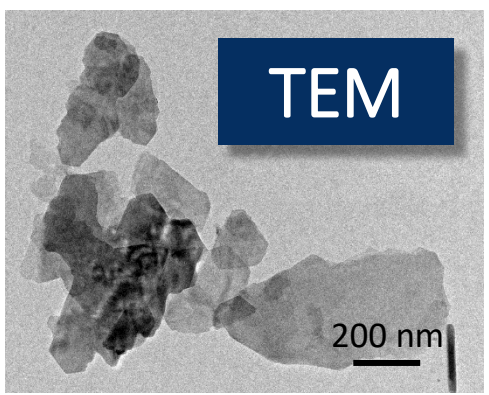

The analysis of large nanomaterials with only one dimension in the range of nanometers (nanoclays) by SP-ICP-MS is proposed

Exploring the boundaries in the analysis of large particles by single particle inductively coupled plasma mass spectrometry: Application to nanoclays

David Ojeda, Eduardo Bolea*, Josefina Pérez-Arantegui, Francisco Laborda

Group of Analytical Spectroscopy and Sensors (GEAS)

Institute of Environmental Sciences (IUCA)

University of Zaragoza

Pedro Cerbuna 12, 50009 Zaragoza, Spain.

* corresponding author. E-mail: edbolea@unizar.es

Abstract

The analysis of microparticles by single particle inductively coupled plasma mass spectrometry (SP-ICP-MS) requires sample introduction systems that guarantee transport efficiencies similar to those obtained with dissolved standards along the size range covered. The utilization of a nebulisation system based on a linear pass spray chamber and a micronebuliser, is discussed and optimized for the introduction of large inorganic particles. Limitations caused by incomplete ionisation or the counting limit of detectors affecting particle size characterisation are also considered. The procedure developed has been applied to the characterisation of suspensions of a natural clay (kaolinite), with thickness in the range of few nanometers and lateral dimensions up to 1 μm. The application of different sensitivity conditions by the modification of the ion transmission, allowed to cover the whole size range of the suspension monitoring ^{27}Al isotope, and a quantitative mass recovery respect to ICP-MS analysis. Finally, the migration of nanoclays (montmorillonite) from food containers and their detection by SP-ICP-MS are

presented. Results have been compared to those obtained by TEM, showing that nanoclays migrated from the containers in water.

Keywords: single particle detection; ICP-MS; microparticles, natural clays, nanoclays migration, food packing.

1. Introduction

Single particle inductively coupled plasma mass spectrometry (SP-ICP-MS) has become a relevant technique for the analysis of nanomaterials due to its unique capacities regarding detection, characterisation and quantification of nanoparticles [1,2]. The basics can be found elsewhere [3,4]. SP-ICP-MS exhibits high detection capabilities, down to number concentrations of 100 particles mL^{-1} and limits of detection in terms of particle size in the range of 10-20 nm for most nanoparticles [5]. According to the Recommendation from the European Commission (2011/696/EU), the definition of nanomaterial is not only considered for spherical particles with diameters below 100 nm, but also for particles in which one or more external dimensions are in that size range [6]. This is the case of the nanoclays: materials that show sheet structures of aluminosilicates with thicknesses in the range of few nanometres, but lateral dimensions that may be extended from tens of nanometres to several micrometres [7].

Due to their mechanical and thermal properties, nanoclays are being used in the production of food containers [8]. Through their incorporation into a polymeric matrix, such as plastics, some of their properties are transferred to the final products, a hybrid commonly denominated nanocomposite. One of the major advantages of these nanocomposites is the barrier effect [9,10], together with the increment of the physical and mechanical resistance, biodegradable capacities and protection against corrosion

[11,12]. Due to all these advancements, the application of nanoclays has raised significantly, along with the interest in the analysis of their structure and their interaction with polymers [7]. Their analysis by SP-ICP-MS, however, may pose relevant limitations because of their dimensions in the micrometre range. When large particles are analysed, difficulties during their transport to the plasma, their incomplete vaporisation/ionisation once reached the plasma or the production of signals out of the range of the detector must be considered [13].

The transport of the particles can be studied through the nebulisation efficiency, defined as the ratio of the amount of analyte entering the plasma to the amount of analyte aspirated. According to the following expression [14]:

$$f_{NP} = \eta_{neb}\, Q_{sam} N_{NP} \qquad \text{(Eq. 1)}$$

the frequency of the nanoparticles detected (f_{NP}) depends on the analyte nebulisation efficiency (η_{neb}) and the sample introduction flow rate (Q_{sam}) respect to the concentration of nanoparticles in number (N_{NP}). Number concentration can be derived by direct calibration, using reference test materials characterised for particle number concentration. The need for the nebulisation efficiency term lies in the difference between the mass transport of a particle along the sample introduction system as compared to that of dissolved ions in solution [15]. The nebulisation efficiency will also vary depending on the size of the particles, as it was examined in the analysis of slurries in ICP-MS systems, in which a decrease in nebulisation efficiencies was found for particles above 2-3 μm [16], and no contribution to the analyte signals for particles above 7-10 μm [17,18].

The efficiency values are dependent on the components of the sample introduction system, apart from other operational parameters, such as the nebuliser gas or the sample uptake flow rates [15,19]. For the analysis of nanoparticles, the most commonly used

systems consist of concentric nebulisers coupled to double pass or cyclonic spray chambers, with transport efficiencies reported ranging from 1 to 10% by applying sample flow rates of 0,1-1 mL min^{-1} [15,20–22]. In order to improve these values, one possibility is the use of low uptake flow rates of some μL min^{-1} [23,24]. The use of a micronebulisers in combination with linear-pass spray chambers, as those used for single cell analysis, has shown nebulisation efficiency improvements for Au NPs (in one order of magnitude respect to cyclonic chambers) [25], but also for polystyrene (PS) beads of 2.5 μm (up to 30% of improvement) [26]. PS particles up to 4-5 μm have been nebulised, with transport efficiencies over 30% for particles of 2 μm by Laborda et al. [27]. Alternatively, it is possible to increase the transport efficiency by the use of direct injection systems, for which the sample containing the particles is directly nebulised into the plasma with no need for spray chambers [28,29]. Among them, the micro-droplet generator is highlighted as the main option [30]. Despite its advantages, direct nebulisation does not guarantee the absence of losses in transport efficiency, which, in addition to the difficulties in its optimisation and in terms of sensitivity and reliability, has limited its applications so far [23,31].

Limitations related to the intensity of the signals corresponding to individual particles are also expected. These limitations lead to non-linear relationships between the signal intensity obtained and the mass (and subsequently size) of one particle, which means an underestimation in its characterisation. The loss of information for large particles was firstly reported by Degueldre et al., when the upper size limits measurable were studied for ZrO_2 and UO_2 colloids, determined in 1-2 μm [32] and 2-6 μm [33], respectively. Non-linear responses have been also shown in the analysis of different nanomaterials, such as Au [34] and SiO_2 particles [21,35]. In general, deviation from linearity can be

explained by two different factors: the degree of vaporisation of the particles and limitations in the detector response [34].

The magnitude of the SP-ICP-MS signal is related to the process of vaporisation of a particle and its production of atomic ions [35]. In turn, the vaporissation/ionisation of the particles depends mainly on the residence time within the plasma, that will require to be longer for larger particles; otherwise, its ionisation may be only partial [13,34]. In addition, larger particles may cause local cooling of the plasma, affecting the fraction of ions generated and transmitted to the mass spectrometer [35]. The linear size range measurable will not be the same for all the particles, since their response may not be equal, depending on their nature. For Au particles, Lee et al. [34] developed a simulation regarding the duration for particle vaporisation/ionisation, concluding that a different behaviour between particles of 100 nm and 250 nm would be expected. In the case of SiO_2 particles, the range is shifted to a larger size, reaching a maximum at 1-2 μm [21,35], from which the intensity response did not correspond to the volumes expected for such sizes, since they can exceed the limit of the pulse-counting mode of the ICP-MS detector [34,36]. In this regard, the linear dynamic range in SP-ICP-MS is often restricted to 3 orders of magnitude in particle mass, which is even more limited in terms of particle diameter, with only 1 or 2 orders of magnitude because of the upper limit in the detector response [13].

In addition to the difficulties caused by their geometry, the analysis of nanoclays may present some other types of limitations by SP-ICP-MS. In the case of its characterisation using Al, the lack of certified materials or size standards of Al_2O_3 particles prevents concrete determinations on nebulisation efficiencies for clay particles based on their size. As an alternative, there is a wide range of size standards of SiO_2 or Si-based particles available. However, the analysis of Si by ICP-MS is limited by the presence of polyatomic

interferences present in the plasma (such as $^{14}N^{14}N^{+}$ or $^{12}C^{16}O^{+}$), which will overlap the signal of the most abundant Si isotope (m/z=28) [37]. Common solutions while using quadrupole analysers are the use of collision [38] or reaction cells [39], or configurations such as ICP-MS/MS [37], despite the loss of sensitivity for the ion of interest that these systems involve.

Considering all these factors, the aim of this work is the analysis of nanoclays by SP-ICP-MS, given their current relevance and complexity. For the development of the method based on SP-ICP-MS, Si and Al isotopes have been monitored, using SiO_2 particle size standards and a commercial suspension of Al_2O_3, which allows the study of the size range measurable. The method has been applied to the characterisation of a suspension of a natural clay (kaolin), whose results are compared to those obtained by Transmission Electron Microscopy (TEM). Finally, given the application of clays in food packaging for the production of nanocomposites, their migration from two different materials containing this kind of particles is studied.

2. Experimental

2.1. Instrumentation

A NexION 2000B ICP mass spectrometer (Perkin Elmer, Toronto, Canada) was used for the single particle analysis. Two different systems for the sample introduction were studied: a cyclonic spray chamber with a concentric glass nebuliser (Meinhard, Colorado, USA), and a linear pass spray chamber (Asperon™, Perkin Elmer) equipped with a flow focusing nebuliser (Ingeniatrics, Sevilla, Spain). Data acquisition and instrumental parameters utilised in single mode for both systems are listed in Table 1.

Table 1. Instrumental and data acquisition parameters used in SP-ICP-MS.

Instrumental parameters		
Spray chamber	cyclonic	linear pass
RF power	1600 W	1600 W
Argon gas flow rate		
Plasma	15 L min^{-1}	15 L min^{-1}
Auxiliary	1.2 L min^{-1}	1.2 L min^{-1}
Nebuliser	1.0 L min^{-1}	1.0 L min^{-1}
Make-up	—	0.2 L min^{-1}
Sample introduction flow rate	370 µL min^{-1}	13 µL min^{-1}
Nebulisation efficiency	5.5 ± 0.1%	41.8 ± 0.4%
Data acquisition parameters		
Dwell time	100 µs	
Total acquisition time	60 s	
Isotopes monitored	^{27}Al or ^{29}Si	

The determination of the total aluminium contents in the samples was performed with the same ICP-MS system in conventional mode. In this case, the cyclonic chamber with the concentric glass nebuliser was used, under the same instrumental conditions specified in Table 1. Dwell time of 50 ms and 20 sweeps per replicate were used for the data acquisition. The isotope monitored was ^{27}Al, using ^{45}Sc as internal standard.

TEM images were obtained using a FEI Tecnai F30 microscope (FEI Technologies Inc., USA) with a Field-Emission Gun (FEG) working at voltages of 200 and 300 KV. The microscope was equipped with a High-Angle Annular Dark-Field detector (HAADF) for Z contrast images, with an Energy Dispersive X-Ray Spectrometer (EDS) for X-ray microanalysis and an energy filter (Gatan Tridiem, USA) for Electron Energy Loss

Spectroscopy (EELS) and Energy-Filtered Transmission Electron Microscopy (EFTEM) analysis. The EDS system was used for the elemental analysis of the samples and EELS for the thickness determination of the particles. The calculation of the absolute and the relative values of the thickness for one sample, from the EELS low-loss spectra, were made through three different methods available in the EELS software (DigitalMicrograph, Gatan Inc., USA): log-ratio (absolute), log-ratio (relative) and the Kramers-Kronig's rule of sum [40].

For the TEM analysis of the materials, few drops of a suspension were deposited on the copper-grid sample holder and dried before its carbon coating for the improvement of their conductivity. The coating was performed with a Leica EM SDC500 vacuum equipment (Leica Microsystem, Viena, Austria).

The dimensions of the particles obtained from the TEM images were determined with the digital imaging processing tool ImageJ, version 1.8.0 (National Institute of Health, USA).

2.2. Standards, particle suspensions and solutions

Throughout the method development, different particle size standards of SiO_2 were used, being all of them supplied as suspensions. The standards of 150 and 2000 nm of nominal size were purchased from Sigma Aldrich (Buchs, Switzerland), whereas the standards of 300, 500 and 1000 nm were obtained from NanoComposix (San Diego, USA). In the case of the aluminium, a suspension of Al_2O_3 particles was utilised with sizes of 30-60 nm (Sigma Aldrich).

Nebulisation efficiencies were determined by using a standard suspension of gold nanoparticles (certified nominal diameter of 49.9 ± 2.2 nm), purchased from NanoComposix. Calculations were made by using the frequency method [15].

For their analysis by SP-ICP-MS, suspensions were diluted in ultrapure water obtained from a Milli-Q purification system equipment (Millipore Co., Bedford, USA). The dilutions were prepared by weight. Before their analysis, suspensions were bath sonicated (P Selecta, Ultrasons, Barcelona, Spain) for 5 min.

The calibration solutions for the determinations of Si and Al, as well as the solution for the internal standard of Sc, were prepared from standards of 1000 mg L^{-1} for each element (Panreac, Barcelona, Spain). In the case of Si, the solutions were diluted in ultrapure water, whereas for the Al and Sc they were prepared in HNO_3 1% (v/v) (J.T. Baker, Netherlands).

2.3. Nanoclays and nanocomposites

Nanoclays analysed along this work were natural kaolin, used as a reference clay, and montmorillonite, one of the most frequently used clays in the packaging sector due to its high surface area and its compatibility with plastics [7,41].

In the case of the kaolin, the material is a solid powder provided by Laboratorios Enosán S.L. (Zaragoza, Spain), with particle size up to 100 μm, although SP-ICP-MS analysis were carried out in suspensions prepared in ultrapure water from the fraction below 1 μm, isolated following the procedure described in the Supplementary Information (Section S1). Kaolinite ($Al_2Si_2O_5(OH_4)$) was the main crystalline structure according to its analysis by X-ray diffraction. The density of the clay is 2.6 g cm^{-3} and the mass fractions for Al and Si of 18.0 and 21.7, respectively.

Montmorillonite $(Na,Ca)_{0,33}(Al,Mg)_2(Si_4O_{10})(OH)_2 \cdot nH_2O$) was analysed in suspensions from migration tests performed with two different nanocomposites supplied by the Technological Institute of Packaging, Transport and Logistics (ITENE, Valencia, Spain): bottles (referred as material #1) and food containers (material #2) of polyethylene

terephthalate (PET). The density of this clay is 2.8 g cm^{-3} with an aluminium mass fraction of 11.7%.

2.4. Migration tests

Two different media were utilised in the migration tests with material #1: ultrapure water and acetic acid 3% (v/v), which are two common food simulants included in the UNE-EN 13130-1 norm [42]. The tests consisted in the suspension of a piece of material #1 (dimensions of 2.5 x 5 cm) in the pertinent solution (contact surface: 25 cm^2). Suspensions were prepared in triplicate for each migration solution tested, keeping in agitation by using a rotatory agitator for 24 hours.

For the food container (material #2), the migration tests followed the procedure described in the EU Regulation No. 10/2011 on plastic materials and articles intended to come into contact with food [43]. Only acetic acid 3% (v/v) was utilised as food simulant in these tests. The whole container was filled with 200 mL of the migration solution. The migration procedures were made in triplicate. Samples remained 10 days in laboratory oven at 60ºC of temperature, after which suspensions were transferred to 50 mL polypropylene (PP) tubes for their analysis.

For both type of tests, the solutions were analysed by SP-ICP-MS and TEM with no further dilution. In the case of Al quantification by ICP-MS, it was required an additional treatment for the digestion, described in the next section.

2.5. Total Al determination by ICP-MS

Natural kaolin and material #1 samples containing nanoclays were digested for the determination of the total Al contents by ICP-MS. The digestion followed the procedure described by Gaines [44], proposed for the elemental analysis of zeolites by ICP-OES but

successfully implemented for the Al determination in aluminosilicates [45,46]. Details on the procedure can be found in SI (Section S2).

Matrix effects were observed even at 1:100 dilution, so the analyses were performed by standard addition calibration. The whole process was validated by comparing the results of the total Al contents in the kaolin determined by ICP-MS to those obtained by X-ray fluorescence (XRF). The aluminium in the sample was 18.0 ± 2.4% (m/m), in agreement with the content determined by XRF (17.1%), verified by t-test (95% confidence interval). Furthermore, a recovery test was made, in which a known concentration of an Al standard solution was added at the beginning of the procedure, with a result of 94 ± 2% recovered.

2.6. Data processing in SP-ICP-MS

A 5 sigma (5σ) criterion was applied along the work for peak detection by SP-ICP-MS. The determination of the size and number concentration detection limits was based on the equations described by Laborda et al. [5], being the size LOD expression equal to the critical value in size (X_C^{size}). A detailed description of these calculations can be found in Section S3 of SI.

All the data obtained from the analysis by SP-ICP-MS were processed using the Syngistix Nano Application software (version 2.5, Perkin Elmer) and the OriginPro 2019b analysis program (OriginLab Corporation, Northampton, USA).

3. Results and discussion

3.1. Nebulisation and detection of microparticles by SP-ICP-MS: SiO_2 particles

Typical nebulisation efficiencies range from 1 to 5% for conventional systems (e.g., using concentric nebulisers and cyclonic spray chambers), although they can be much higher for high-efficiency nebulisation ones. These values not only depend on the components, but also on various operational parameters, so the transport efficiency can vary across different instruments or operational setups [15]. Throughout this work, two different setups, working under optimal conditions, were tested. A conventional cyclonic spray chamber equipped with a concentric nebuliser was used as reference; whereas a linear pass spray chamber (Asperon™), originally developed for the introduction of cells and successfully applied for the nebulisation of microplastics [27], was used in combination with a flow focusing nebuliser. This latter setup allows to obtain nebulisation efficiencies up to 40% at sample flow rates around 15 μL min^{-1}, whereas the first one is designed to work at ca. 0.4 mL min^{-1}.

As a first approximation to nanoclays and due to the unavailability of standards for analytical uses, SiO_2 particles were selected. Silicon isotopes are subjected to a number of significant polyatomic interferences. Although the use of collision/reaction cells in conventional ICP-MS allows to improve detection limits, their inherent loss of sensitivity in combination with the peak broadening observed in SP-ICP-MS [47], affect negatively to size detection limits. In view of these constrains, Montaño et al. [48] confirmed that, for measuring silicon by SP-ICP-MS, the use of dwell times in the microsecond range was a better option than using collision/reaction cells for reducing the background from polyatomics. For these reasons, no collision/reaction gases were used in this work while measuring at 100 μs dwell times. Table 2 summarises the figures of merit obtained with the two sample introduction setups studied.

Table 2. Figures of merit obtained for both chambers by SP-ICP-MS for the analysis of SiO_2 particles. Blank intensities and number of events expressed as mean ± s (n=3).

Spray Chamber	Isotope	Sensitivity (counts per µg L^{-1})	Blank intensity (counts)	Blank events	LOD_{number} (mL^{-1})	LOD_{size} (nm)	Maximum size (nm)
Cyclonic	^{28}Si	0.46	75 ± 11	11 ± 4	1.17×10^3	270	500
	^{29}Si	0.18	21 ± 6	15 ± 3	1.60×10^3	300	<1000*
Linear pass	^{29}Si	0.04	28 ± 14	5 ± 3	2.61×10^3	425	1200

* Value estimated. Nebulisation efficiencies for SiO_2 particles of 1000 nm are much lower than those observed for 500 nm particles with the cyclonic chamber.

Although ^{28}Si is the most abundant silicon isotope and hence the most sensitive, this can be a drawback for detection of large particles if the intensity of the particle events exceeds the count rate limit of the electron multiplier detector. For the instrument used throughout this work, this limit was 1560 counts, operating in single particle mode and using a dwell time of 100 µs. Under such conditions, with the cyclonic spray chamber, ^{28}Si could be used to measure SiO_2 particles up to 500 nm, whereas ^{29}Si was selected for measuring larger particles, but smaller than 1000 nm due to low nebulization efficiencies observed at that size range, as discuss below. In the case of the linear pass spray chamber setup, that limit of the detector would be established in 1200 nm for SiO_2 particles for ^{29}Si (see Section S4 for a detailed description of the calculations).

As it is shown in Table 1, the cyclonic spray chamber setup showed lower nebulisation efficiency than the linear pass one when checked with nanoparticles, although its overall transport rate (number concentration x nebulisation efficiency x sample flow rate) was 3.8 times lower. However, when SiO_2 particles of 1000 nm were nebulised with the cyclonic spray chamber, the nebulisation efficiency dropped more than 4-fold, whereas with the linear pass spray chamber setup it remained similar. This was not the case when nebulising particles of 2000 nm, whose nebulisation efficiency fall below 2%, in contrast

to polyethylene microparticles of the same size which are nebulised in a similar way than nanoparticles or dissolved species [27], pointing out the relevance of the particle density on its nebulisation. Therefore, it can be stated that the use of the linear pass spray chamber setup improved the introduction of large SiO_2 particles up to ca. 1 μm in terms of nebulisation efficiency and it should be the chosen option when analysing nanoclays that may show one dimension in the micrometre range.

A 5-sigma criterion was selected for particle discrimination and estimation of size detection limits, as described in [5]. Size detection limits ranged from 270 to 300 nm with the cyclonic chamber, to 425 nm with the linear pass spray chamber setup. The combination of the relatively high intensity of the baseline signal due to polyatomic interferences, together with the fluctuations caused by the peristaltic pump when delivering flows at 13 μL min^{-1}, justified the higher size detection limits observed for the linear pass spray chamber system. Application of a 5-sigma discrimination criterion allows the reduction of the occurrence of false positives when counting particles by SP-ICP-MS on the blanks (5 ± 3 counts with the linear pass spray chamber setup), maintaining the number detection limits in the range of 10^3 particles mL^{-1}.

3.2. Microparticle size determination: Signals obtained from SiO_2 particles

The size of particles does not only affect the efficiency of their transport to the plasma, as discussed in the previous section, but also the efficiency of the plasma to vaporise, atomise, and ionise the particles themselves. Whereas the number of particle events detected is related to their nebulisation efficiency, their intensity depends on the vaporisation and ionisation efficiencies obtained for the particles [27].

Although the size of the particles can be determined through interpolation of the intensity of particle events detected with a calibration performed from particle size standards of the same composition and shape of the particles detected, they can be also estimated from a calibration with dissolved standards of the element monitored, once the nebulisation efficiency and the sample flow rate are known, and the element in dissolved and particulate forms behaves in the plasma in the same way. Figure S5 in SI shows the plot of the mean intensity of particle events vs. the cubed diameter of SiO_2 particles in the range of 500-2000 nm. A slope of 2.83 ± 0.04 was obtained, close to theoretical expected value of 3, although showing a relevant deviation of 25% lower than expected for 2000 nm particles with respect to the rest of standards, suggesting the partial vaporisation of these particles with respect to the smaller ones. This result is in agreement with the work by Lee et al.[34], who observed a linear trend for SiO_2 particles up to 1000 nm.

3.3. Analysis of kaolin nanoclays under the use of ^{27}Al

Under the conditions studied, the upper size limit for SiO_2 particles was established between 1000 and 2000 nm. Above this size, the trueness of the analysis is limited by nebulisation and ionisation issues, which could not be overcome with the available systems. On the other hand, the lower size limit depends on the intensity of the baseline and its associated noise, resulting in a size detection limit of 425 nm for SiO_2 spherical particles. Assuming similar plasma processes for aluminosilicates and silica, the upper size limit should be similar, although the use of the ^{27}Al instead of ^{29}Si for analysis could improve the limits of detection in size. Since there are no relevant contributions from polyatomic interferences at mass 27, baseline intensity was significantly lower (below 1 count) for ^{27}Al, being due to residual aluminium contamination. As a result, together with a higher sensitivity for aluminium (26.30 vs. 0.04 counts per μg L^{-1} in the present work),

the size detection limit achieved was of 35 nm for Al_2O_3 particles, maintaining the number concentration detection limits in 10^3 particles mL^{-1}.

The analysis of a commercial suspension of Al_2O_3 particles with a nominal size distribution ranging from 30 to 60 nm showed good agreement with the supplier, obtaining a size distribution from the size limit of detection (35 nm) up to 70 nm, as can be seen in SI (Section S6).

The procedure was then applied to a natural clay (kaolin), in which the aluminosilicate particles below 1 μm had been isolated to ensure their transport and complete vaporisation and ionisation to the plasma, according to Sections 3.1 and 3.2. Size distributions obtained for ^{27}Al are reported in Figure 1a. Because particles of kaolinite present laminar structures, size is measured as equivalent diameter (estimated diameter of a spherical particle with the same composition, mass and density of a natural one). Kaolinite particles with equivalent diameters from 35 nm up to 420 nm were detected. The upper size limit corresponds to the maximum count rate measured by the detector in single particle mode, determined in a similar way to the determination of SiO_2 particles (see Section S4 in SI).

The kaolinite suspensions were analysed by TEM and EELS to obtain the dimensions of the particles observed. Figure 1b shows the size distributions obtained from the TEM images (number of particles counted = 60), corresponding to the projected areas of the particles assuming a disk shape. For the thickness, estimations of 50 nm for individual sheets and 80 nm for aggregates were established by EELS (see Section S7 in SI). Some similarities can be established in the size range when these two distributions are compared, as shown in Figure 1, with no presence of a small fraction of particles below the critical value applied. However, it was observed that a fraction above 420 nm up to 900 nm was not detected by SP-ICP-MS. The evidence of an undetected fraction of particles was confirmed by quantifying the total aluminium content in the suspensions

from the SP-ICP-MS data, which accounted for the 21% of the aluminium determined by ICP-MS after acid digestion.

To prove that the undetected fraction was a matter of the detector upper dynamic range, sensitivity was decreased by reducing the transmission of ions through the ion optics, so the signal from larger particles would not exceed the detector range. The voltage of the deflector quadrupole, used for bending and focusing the ion beam in the instrument, was modified from the optimised conditions of highest transmission of -13.25 V to -1.75 V, allowing the detection of large particles up to 1000 nm, as can be seen in Figure 2. The reduction in sensitivity led to a shift in the measurable range, losing information related to the smaller fraction, due to the increase of the size detection limit to 110 nm, with the consequent reduction of the number of events registered and, hence, the number concentration of kaolinite particles, as summarized in Table 3.

Table 3. Results for the analysis of the fraction below 1 μm from kaolin using the isotope ^{27}Al, depending on the deflector voltage and as a combination of these two conditions. Results expressed as mean ± s (n = 3).

Deflector voltage	**Al sensitivity (counts per μg L^{-1})**	**Al mass concentration in distribution (μg L^{-1})**	**No. of events**	**Kaolinite particle number concentration (mL^{-1})**
-13.25 V	26.32	1.13 ± 0.07	3175 ± 165	$5.85\times10^5 \pm 0.31\times10^5$
-1.75 V	0.15	6.23 ± 0.36	2240 ± 70	$4.13\times10^5 \pm 0.14\times10^5$
Distributions combined for both deflector voltages		**Al mass concentration in distribution by SP-ICP-MS (μg L^{-1})**		**Al mass concentration by ICP-MS (μg L^{-1})**
		6.26 ± 0.52		5.53 ± 0.34

On the contrary, the detection of larger particles showed a significant increase in terms of Al mass, compensating the low recovery obtained when using the optimised conditions. As it can be shown in Figure 2, by applying these two sets of conditions and combining the corresponding distributions, it was possible to characterise kaolinite particles in a wide range of sizes, from 35 nm to 1 μm. Given the lack of certified materials for the size range analysed, validation of the results in terms of size distributions could not be achieved beyond their comparison to TEM results. For the whole range detected by SP-ICP-MS, Al mass concentration was 6.3 μg L^{-1}, which implies a quantitative recovery respect to the results quantified by ICP-MS, as shown in Table 2. This result suggests that nebulisation and ionisation issues previously discussed could be circumvented using different sensitivity conditions to cover the whole size distribution, with fair mass recoveries for the characterisation of nanoclays such as kaolinite in the range described (up to 1 μm).

3.4. Detection and characterisation of nanoclays migration from plastic containers

The incorporation of nanoclays into plastic matrices to produce nanocomposites in food industry has evidenced the need for studies regarding its potential risk in human health. When used, the main route of exposure for nanoclays is via migration from containers to the food [41]. For this reason, migration studies have always involved the use of food simulants, following procedures according to EU Regulation 10/2011 or UNE-EN 13130-1 for plastic materials and articles intended to be in contact with food. In these norms, the determination of limits for global substances migrated does not specify in what forms, with no restrictions for particles [49]. As a result, the evaluation of nanomaterials migrated is commonly based on total element quantification by ICP-OES or ICP-MS [50–55]. In the case of nanoclays, only a few studies carried out include specific information

for particles, in which only their presence could be confirmed by Scanning Electron Microscopy [56] or SP-ICP-MS [57].

The SP-ICP-MS procedure developed was firstly applied to the material #1, in which montmorillonite is incorporated (see Section 2.3). For the migration tests, two of the main food simulants according to UNE-EN 13130-1 regulation were studied: ultrapure water and acetic acid 3% (v/v), following the procedure described in Section 2.4. The use of acetic acid allows to acidify the migration conditions to simulate a more aggressive scenario than ultrapure water [58]. However, it was observed that this medium leads to higher baseline intensities for ^{27}Al than ultrapure water, as well as the detection of more particle events, which produced higher limits of detection in both size and number concentration for montmorillonite particles, with values of 98 nm and 7.4×10^3 particles mL^{-1}, respectively. Under these conditions, the analysis of migration in acetic acid from material #1 resulted in no detection of particles.

Using ultrapure water as food simulant, the limits of detection improved to levels of 65 nm in size and 4.7×10^3 particles mL^{-1} in number concentration, which allowed the detection of particles from 65 to 300 nm in the migration samples. Size distribution is shown in Figure 3, with particles below 100 nm as the most frequent equivalent diameter. Although samples were also analysed by TEM, only a low number of particles were observed, in most cases with sizes of several micrometres and high carbon contents (see Section S8 in SI). Inside these microfragments, they were embedded some hexagonal structures, whose EDS spectra confirmed the presence of aluminium and silicon that would belong to the aluminosilicate particles added into the material #1. Due to the lack of isolated particles detected by TEM, it was not possible to estimate the thickness of the montmorillonite particles. If a value of 50 nm is considered, as it was the case for kaolinite, the hexagonal structures would result in 70-125 nm of equivalent diameter,

which would be in agreement with the size distributions obtained by SP-ICP-MS. The results suggest that what actually migrate from material #1 are the microfragments of plastic with the nanoclays embedded. However, this cannot be confirmed, due to the scarce number of particles observed by TEM.

In material #2, the migration of montmorillonite was tested using acetic acid 3% (v/v) as simulant, according to the procedure specified by EU Regulation 10/2011 (see Section 2.4). This regulation has been followed by several former studies regarding the migration of both nanoparticles [59,60] and clays [58].

As seen for material #1, the use of acetic acid 3% also led to a worsening of the SP-ICP-MS performance, with LOD in size and in number concentration of 110 nm and of 5.2×10^3 particles mL^{-1}, respectively. In such conditions, it was not possible to detect particles above the limits of detection when the procedure was applied to the migration suspensions from the container. A small number of particles of several micrometres were observed by TEM, in which Al and Si were present. Comparing to the total Al determined by ICP-MS (22 ± 2 μg L^{-1}), similar concentrations were quantified by SP-ICP-MS (20 ± 3 μg L^{-1}). The results confirmed that quantification by SP-ICP-MS was correct (verified by *t-test*, 95% confidence interval), with practically all the aluminium present in dissolved forms, and no relevant contribution in terms of mass from particles. Along with the migration tests from material #1, the results indicated that the use of acetic acid 3% may lead to the possible dissolution of the aluminosilicate particles migrated, causing the low number concentration of particles detected and the high levels of dissolved aluminium, in comparison to a softer medium such as ultrapure water.

4. Conclusions

The detection and characterisation of particles in a wide range of sizes by SP-ICP-MS is still problematic, especially when dealing with particles in the range of micrometres. The efficiency of the introduction of these particles into the plasma should not be given for granted compared to that of dissolved species or smaller nanoparticles, even under optimised conditions. The lack of reliable standards in this range of sizes makes difficult the assessment of the actual nebulisation efficiency of large particles. The use of well-characterised SiO_2 suspensions has shown that transport efficiencies are reduced as long as the particle size reaches the range of 1 μm. Therefore, the use of strategies based on nanoparticles size standards for calibration may lead to the underestimation of number concentrations for large particles. Besides, even if nebulisation efficiency is estimated with these large standards, it is possible that particles with different shape, such as nanoclays, with a sheet form, show a different behaviour. In this work, a mass recovery assay, together with a comparison through the analysis by TEM are proposed to validate the results obtained by SP-ICP-MS, as shown for a kaolinite suspension. The use of Al instead of Si to detect aluminosilicates allows to broaden the working range at low sizes. On the other hand, the upper size limit is also conditioned by the detector response used in ICP-MS instruments. The selection of different experimental conditions to modulate the sensitivity can also be used to modify the size range. The application of two different deflector voltages has been used to cover the whole size range observed for the kaolin suspension. Finally, the procedure has proved to be useful in the detection of nanoclays (montmorillonite) migrating from packing materials in different migration tests.

Conflicts of interest

There are no conflicts of interest to declare

Acknowledgments.

This work was supported by the Spanish Ministry of Science, Innovation and Universities and the European Regional Development Found, project RTI2018-096111-B-I00 (MICINN/FEDER) and the Government of Aragon (E29_17R). Authors would like also to acknowledge to the Technological Institute of Packaging, Transport and Logistics (ITENE, Valencia, Spain), for providing the nanocomposites, to the Servicio General de Apoyo a la Investigación-SAI, Universidad de Zaragoza, and to Laboratorio de Microscopías Avanzadas (LMA) - Universidad de Zaragoza (especially to Rodrigo Fernández-Pacheco for EELS measurements).

Figure captions

Figure 1. Size distributions for fraction below 1 μm from kaolin obtained by: a) SP-ICP-MS for ^{27}Al isotope and b) TEM. Sizes are referred as equivalent diameters of kaolinite, considering particles as spheres. Equivalent size for the critical value applied in SP-ICP-MS analysis (X_C^{size}) of 35 nm.

Figure 2. Size distributions for fraction below 1 μm from kaolin depending on the deflector voltage applied in SP-ICP-MS. Sizes are referred as equivalent diameters of kaolinite, considering particles as spheres. Equivalent sizes for the critical value applied

in SP-ICP-MS analysis (X_C^{size}) of 35 nm and 110 nm for voltages of -13.25 V (optimised conditions) and -1.75 V, respectively.

Figure 3. Size distributions of particles migrated from material #1 in ultrapure water as medium. Sizes are referred as equivalent diameters of montmorillonite, considering particles as spheres. Equivalent size for the critical value applied in SP-ICP-MS analysis (X_C^{size}) of 65 nm.

Figure 1

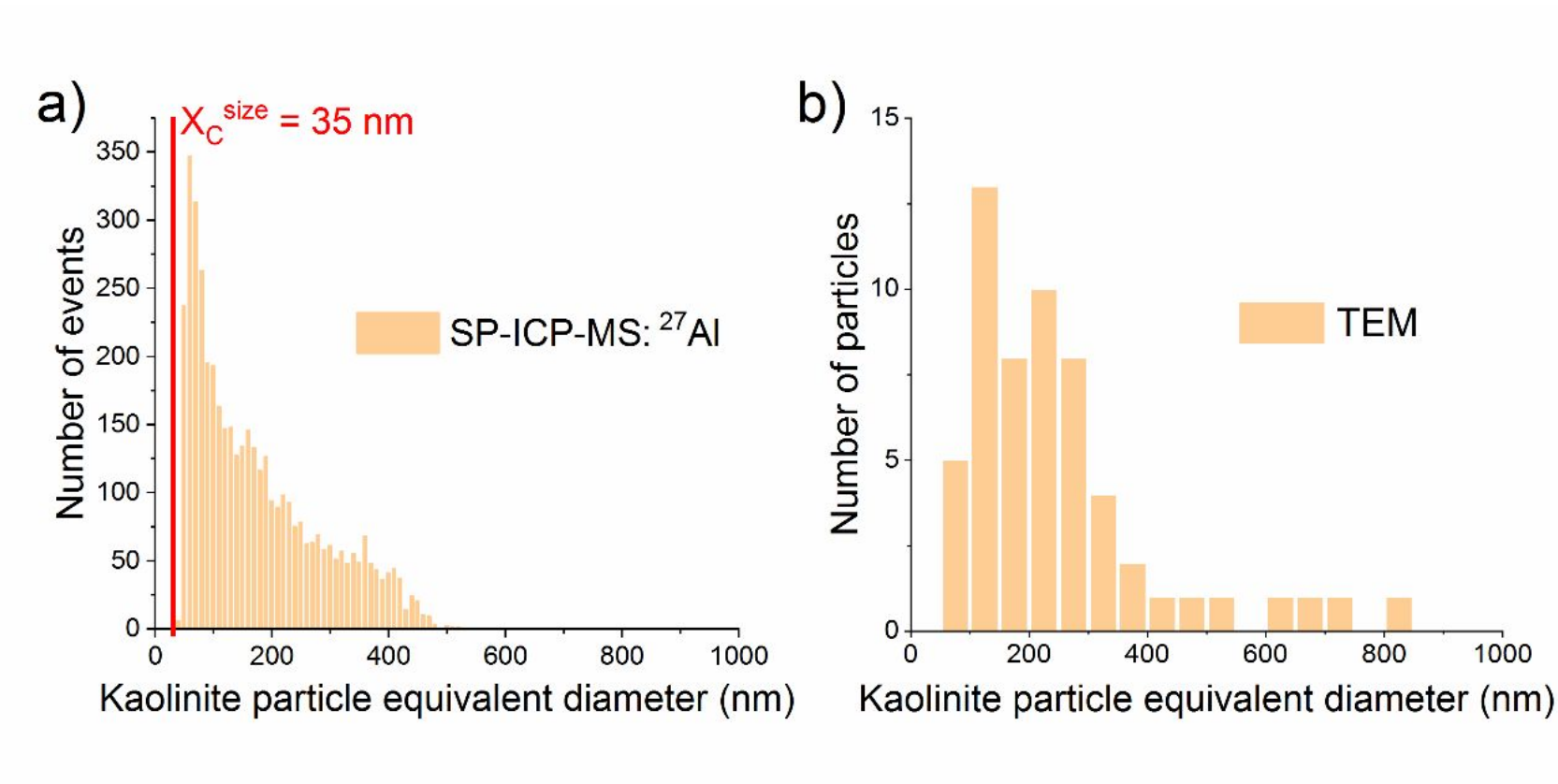
a)
X_C^{size} = 35 nm
Number of events
SP-ICP-MS: ^{27}Al
Kaolinite particle equivalent diameter (nm)
b)
Number of particles
TEM
Kaolinite particle equivalent diameter (nm)

Figure 2

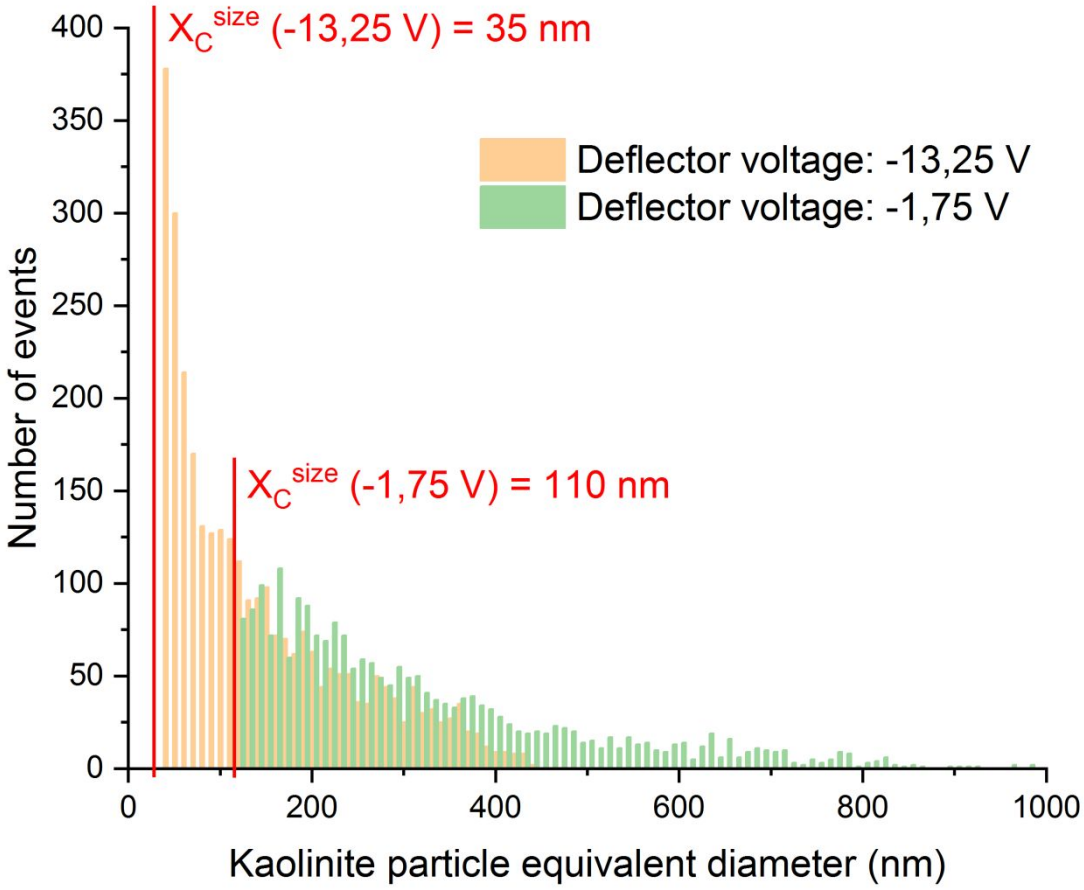
X_C^{size} (-13,25 V) = 35 nm
Deflector voltage: -13,25 V
Deflector voltage: -1,75 V
X_C^{size} (-1,75 V) = 110 nm
Number of events
Kaolinite particle equivalent diameter (nm)
0
50
100
150
200
250
300
350
400
0
200
400
600
800
1000

Figure 3

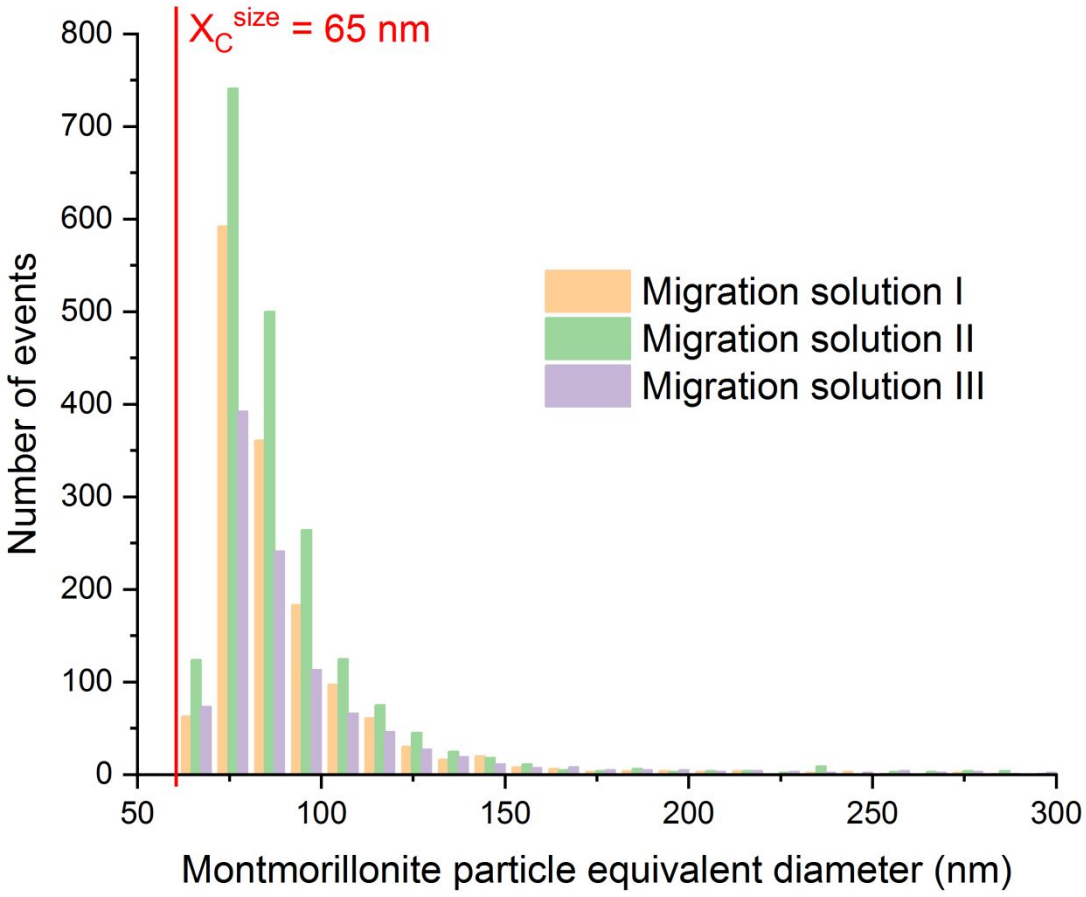
X_C^{size} = 65 nm
Number of events
Montmorillonite particle equivalent diameter (nm)
Migration solution I
Migration solution II
Migration solution III
0
100
200
300
400
500
600
700
800
50
100
150
200
250
300

References

[1] A.R. Donovan, C.D. Adams, Y. Ma, C. Stephan, T. Eichholz, H. Shi, Fate of nanoparticles during alum and ferric coagulation monitored using single particle ICP-MS, Chemosphere. 195 (2018) 531–541. https://doi.org/10.1016/j.chemosphere.2017.12.116.

[2] F. Laborda, A.C. Gimenez-Ingalaturre, E. Bolea, J.R. Castillo, Single particle inductively coupled plasma mass spectrometry as screening tool for detection of particles, Spectrochim. Acta - Part B At. Spectrosc. 159 (2019) 105654. https://doi.org/10.1016/j.sab.2019.105654.

[3] C. Degueldre, P.-Y. Favarger, Colloid analysis by single particle inductively coupled plasma-mass spectroscopy: a feasibility study, Colloids Surfaces A Physicochem. Eng. Asp. 217 (2003) 137–142. https://doi.org/10.1016/S0927-7757(02)00568-X.

[4] E. Bolea, J. Jiménez-Lamana, F. Laborda, J.R. Castillo, Size characterization and quantification of silver nanoparticles by asymmetric flow field-flow fractionation coupled with inductively coupled plasma mass spectrometry, Anal. Bioanal. Chem. 401 (2011) 2723–2732. https://doi.org/10.1007/s00216-011-5201-2.

[5] F. Laborda, A.C. Gimenez-Ingalaturre, E. Bolea, J.R. Castillo, About detectability and limits of detection in single particle inductively coupled plasma mass spectrometry, Spectrochim. Acta - Part B At. Spectrosc. 169 (2020) 105883. https://doi.org/10.1016/j.sab.2020.105883.

[6] European Commission 2011/696 on the definition of nanomaterial, Off. J. Eur. Union. 24 (2011) 6–6. https://doi.org/10.7748/ns.24.26.6.s4.

[7] M. Farhoodi, Nanocomposite Materials for Food Packaging Applications: Characterization and Safety Evaluation, Food Eng. Rev. 8 (2016) 35–51. https://doi.org/10.1007/s12393-015-9114-2.

[8] B.C. Ku, D. Froio, D. Sleeves, D.W. Kim, H. Ahn, J.A. Ratio, A. Blumstein, J. Kumar, L.A. Samuelson, Cross-linked multilayer polymer-clay nanocomposites and permeability properties, J. Macromol. Sci. - Pure Appl. Chem. 41 A (2004) 1401–1410. https://doi.org/10.1081/MA-200035343.

[9] T. V. Duncan, Applications of nanotechnology in food packaging and food safety: Barrier materials, antimicrobials and sensors, J. Colloid Interface Sci. 363 (2011) 1–24. https://doi.org/10.1016/j.jcis.2011.07.017.

[10] J.Y. Huang, X. Li, W. Zhou, Safety assessment of nanocomposite for food packaging application, Trends Food Sci. Technol. 45 (2015) 187–199. https://doi.org/10.1016/j.tifs.2015.07.002.

[11] R. Nosrati, A. Olad, The effect of TiO 2 /aluminosilicate nanocomposite additives on the mechanical and thermal properties of polyacrylic coatings, Appl. Surf. Sci. 357 (2015) 376–384. https://doi.org/10.1016/j.apsusc.2015.09.019.

[12] G. Choudalakis, A.D. Gotsis, Permeability of polymer/clay nanocomposites: A review, Eur. Polym. J. 45 (2009) 967–984. https://doi.org/10.1016/j.eurpolymj.2009.01.027.

[13] B. Meermann, V. Nischwitz, ICP-MS for the analysis at the nanoscale-a tutorial review, J. Anal. At. Spectrom. 33 (2018) 1432–1468. https://doi.org/10.1039/c8ja00037a.

[14] F. Laborda, J. Jiménez-Lamana, E. Bolea, J.R. Castillo, Critical considerations

for the determination of nanoparticle number concentrations, size and number size distributions by single particle ICP-MS, J. Anal. At. Spectrom. 28 (2013) 1220–1232. https://doi.org/10.1039/c3ja50100k.

[15] H.E. Pace, N.J. Rogers, C. Jarolimek, V.A. Coleman, C.P. Higgins, J.F. Ranville, Determining Transport Efficiency for the Purpose of Counting and Sizing Nanoparticles via Single Particle Inductively Coupled Plasma Mass Spectrometry, Anal. Chem. 83 (2011) 9361–9369. https://doi.org/10.1021/ac201952t.

[16] P. Goodall, M.E. Foulkes, L. Ebdon, Slurry nebulization inductively coupled plasma spectrometry-the fundamental parameters discussed, Spectrochim. Acta Part B At. Spectrosc. 48 (1993) 1563–1577. https://doi.org/10.1016/0584-8547(93)80143-I.

[17] L. Ebdon, M. Foulkes, K. Sutton, Slurry nebulization in plasmas, J. Anal. At. Spectrom. 12 (1997) 213–229. https://doi.org/10.1039/a604914a.

[18] Z. Wang, P. Yang, Slurry nebulization in plasmas for analysis of advanced ceramic materials, J. Anal. At. Spectrom. 29 (2014) 2091–2103. https://doi.org/10.1039/c4ja00161c.

[19] M. Loula, A. Kaňa, R. Koplík, J. Hanuš, M. Vosmanská, O. Mestek, Analysis of Silver Nanoparticles Using Single-Particle Inductively Coupled Plasma–Mass Spectrometry (ICP-MS): Parameters Affecting the Quality of Results, Anal. Lett. 52 (2019) 288–307. https://doi.org/10.1080/00032719.2018.1459657.

[20] A.R. Montoro Bustos, E.J. Petersen, A. Possolo, M.R. Winchester, Post hoc Interlaboratory Comparison of Single Particle ICP-MS Size Measurements of NIST Gold Nanoparticle Reference Materials, Anal. Chem. 87 (2015) 8809–

8817. https://doi.org/10.1021/acs.analchem.5b01741.

[21] R. Peters, Z. Herrera-Rivera, A. Undas, M. van der Lee, H. Marvin, H. Bouwmeester, S. Weigel, Single particle ICP-MS combined with a data evaluation tool as a routine technique for the analysis of nanoparticles in complex matrices, J. Anal. At. Spectrom. 30 (2015) 1274–1285. https://doi.org/10.1039/C4JA00357H.

[22] M. Witzler, F. Küllmer, A. Hirtz, K. Günther, Validation of Gold and Silver Nanoparticle Analysis in Fruit Juices by Single-Particle ICP-MS without Sample Pretreatment, J. Agric. Food Chem. 64 (2016) 4165–4170. https://doi.org/10.1021/acs.jafc.6b01248.

[23] F.H. Lin, S.I. Miyashita, K. Inagaki, Y.H. Liu, I.H. Hsu, Evaluation of three different sample introduction systems for single-particle inductively coupled plasma mass spectrometry (spICP-MS) applications, J. Anal. At. Spectrom. 34 (2019) 401–406. https://doi.org/10.1039/c8ja00295a.

[24] Y. Cao, J. Feng, L. Tang, C. Yu, G. Mo, B. Deng, A highly efficient introduction system for single cell- ICP-MS and its application to detection of copper in single human red blood cells, Talanta. 206 (2020) 120174. https://doi.org/10.1016/j.talanta.2019.120174.

[25] E. Mavrakis, L. Mavroudakis, N. Lydakis-Simantiris, S.A. Pergantis, Investigating the uptake of arsenate by chlamydomonas reinhardtii cells and its effect on their lipid profile using single cell ICP-MS and Easy Ambient Sonic-Spray Ionization-MS, Anal. Chem. 91 (2019) 9590–9598. https://doi.org/10.1021/acs.analchem.9b00917.

[26] R.C. Merrifield, C. Stephan, J.R. Lead, Quantification of Au Nanoparticle

Biouptake and Distribution to Freshwater Algae Using Single Cell - ICP-MS, Environ. Sci. Technol. 52 (2018) 2271–2277. https://doi.org/10.1021/acs.est.7b04968.

[27] F. Laborda, C. Trujillo, R. Lobinski, Analysis of microplastics in consumer products by single particle-inductively coupled plasma mass spectrometry using the carbon-13 isotope, Talanta. 221 (2021) 121486. https://doi.org/10.1016/j.talanta.2020.121486.

[28] L. Mueller, H. Traub, N. Jakubowski, D. Drescher, V.I. Baranov, J. Kneipp, Trends in single-cell analysis by use of ICP-MS, Anal. Bioanal. Chem. 406 (2014) 6963–6977. https://doi.org/10.1007/s00216-014-8143-7.

[29] S. Gschwind, M. de L. Aja Montes, D. Günther, Comparison of sp-ICP-MS and MDG-ICP-MS for the determination of particle number concentration, Anal. Bioanal. Chem. 407 (2015) 4035–4044. https://doi.org/10.1007/s00216-015-8620-7.

[30] M. Corte-Rodríguez, R. Álvarez-Fernández, P. García-Cancela, M. Montes-Bayón, J. Bettmer, Single cell ICP-MS using on line sample introduction systems: Current developments and remaining challenges, TrAC - Trends Anal. Chem. 132 (2020). https://doi.org/10.1016/j.trac.2020.116042.

[31] M. Tharaud, P. Louvat, M.F. Benedetti, Detection of nanoparticles by single-particle ICP-MS with complete transport efficiency through direct nebulization at few-microlitres-per-minute uptake rates, Anal. Bioanal. Chem. 413 (2021) 923–933. https://doi.org/10.1007/s00216-020-03048-y.

[32] C. Degueldre, P.-Y. Favarger, C. Bitea, Zirconia colloid analysis by single particle inductively coupled plasma–mass spectrometry, Anal. Chim. Acta. 518

(2004) 137–142. https://doi.org/10.1016/j.aca.2004.04.015.

[33] C. Degueldre, P.-Y. Favarger, R. Rossé, S. Wold, Uranium colloid analysis by single particle inductively coupled plasma-mass spectrometry., Talanta. 68 (2006) 623–628. https://doi.org/10.1016/j.talanta.2005.05.006.

[34] W.W. Lee, W.T. Chan, Calibration of single-particle inductively coupled plasma-mass spectrometry (SP-ICP-MS), J. Anal. At. Spectrom. 30 (2015) 1245–1254. https://doi.org/10.1039/c4ja00408f.

[35] J.W. Olesik, P.J. Gray, Considerations for measurement of individual nanoparticles or microparticles by ICP-MS: Determination of the number of particles and the analyte mass in each particle, J. Anal. At. Spectrom. 27 (2012) 1143–1155. https://doi.org/10.1039/c2ja30073g.

[36] K.S. Ho, K.O. Lui, K.H. Lee, W.T. Chan, Considerations of particle vaporization and analyte diffusion in single-particle inductively coupled plasma-mass spectrometry, Spectrochim. Acta - Part B At. Spectrosc. 89 (2013) 30–39. https://doi.org/10.1016/j.sab.2013.08.012.

[37] E. Bolea-fernandez, D. Leite, A. Rua-ibarz, L. Balcaen, F. Vanhaecke, Characterization of SiO 2 Nanoparticles by Single Particle – Inductively Coupled Plasma – Tandem Mass Spectrometry (SP- ICP-MS / MS), J. Anal. At. Spectrom. (2017) 43–78.

[38] F. Chainet, C.P. Lienemann, J. Ponthus, C. Pécheyran, J. Castro, E. Tessier, O.F.X. Donard, Towards silicon speciation in light petroleum products using gas chromatography coupled to inductively coupled plasma mass spectrometry equipped with a dynamic reaction cell, Spectrochim. Acta - Part B At. Spectrosc. 97 (2014) 49–56. https://doi.org/10.1016/j.sab.2014.04.010.

[39] S. Addo Ntim, S. Norris, K. Scott, T.A. Thomas, G.O. Noonan, Consumer use effects on nanoparticle release from commercially available ceramic cookware, Food Control. 87 (2018) 31–39. https://doi.org/10.1016/j.foodcont.2017.12.003.

[40] R.F. Egerton, Electron Energy-Loss Spectroscopy in the Electron Microscope, Springer New York, 1996.

[41] N. Bumbudsanpharoke, S. Ko, Nanoclays in food and beverage packaging, J. Nanomater. 2019 (2019). https://doi.org/10.1155/2019/8927167.

[42] UNE-EN 13130-1 norm. Materials and articles in contact with foodstuffs, (2005).

[43] Commision regulation (EU) No 10/2011: On plastic materials and articles intended to come into contact with food, Off. J. Eur. Union. (2011).

[44] P. Gaines, Elemental analysis of zeolites, Inorganic Ventures Europe S.L., n.d. http://www.inorganicventures.com/elemental-analysis-zeolites.

[45] T. Williamson, J. Han, L. Katz, G. Sant, M.C.G. Juenger, Method for experimentally determining n-a-s-(H) solubility, RILEM Tech. Lett. 3 (2018) 104–113. https://doi.org/10.21809/rilemtechlett.2018.63.

[46] T. Williamson, L.E. Katz, J. Han, H.A. Dobbs, B.F. Chmelka, G. Sant, M.C.G. Juenger, Relationship between aqueous chemistry and composition, structure, and solubility of sodium aluminosilicate hydrates, J. Am. Ceram. Soc. 103 (2020) 2160–2172. https://doi.org/10.1111/jace.16868.

[47] E. Bolea-Fernandez, D. Leite, A. Rua-Ibarz, T. Liu, G. Woods, M. Aramendia, M. Resano, F. Vanhaecke, On the effect of using collision/reaction cell (CRC) technology in single-particle ICP-mass spectrometry (SP-ICP-MS), Anal. Chim. Acta. 1077 (2019) 95–106. https://doi.org/10.1016/j.aca.2019.05.077.

[48] M.D. Montaño, B.J. Majestic, Å.K. Jämting, P. Westerhoff, J.F. Ranville, Methods for the Detection and Characterization of Silica Colloids by Microsecond spICP-MS, Anal. Chem. 88 (2016) 4733–4741. https://doi.org/10.1021/acs.analchem.5b04924.

[49] C. V. Garcia, G.H. Shin, J.T. Kim, Metal oxide-based nanocomposites in food packaging: Applications, migration, and regulations, Trends Food Sci. Technol. 82 (2018) 21–31. https://doi.org/10.1016/j.tifs.2018.09.021.

[50] B. Panea, G. Ripoll, J. González, Á. Fernández-Cuello, P. Albertí, Effect of nanocomposite packaging containing different proportions of ZnO and Ag on chicken breast meat quality, J. Food Eng. 123 (2014) 104–112. https://doi.org/10.1016/j.jfoodeng.2013.09.029.

[51] Z. Lian, Y. Zhang, Y. Zhao, Nano-TiO2 particles and high hydrostatic pressure treatment for improving functionality of polyvinyl alcohol and chitosan composite films and nano-TiO2 migration from film matrix in food simulants, Innov. Food Sci. Emerg. Technol. 33 (2016) 145–153. https://doi.org/10.1016/j.ifset.2015.10.008.

[52] W. Li, C. Zhang, H. Chi, L. Li, T. Lan, P. Han, H. Chen, Y. Qin, Development of antimicrobial packaging film made from poly(lactic acid) incorporating titanium dioxide and silver nanoparticles, Molecules. 22 (2017). https://doi.org/10.3390/molecules22071170.

[53] M.A. Busolo, J.M. Lagaron, Oxygen scavenging polyolefin nanocomposite films containing an iron modified kaolinite of interest in active food packaging applications, Innov. Food Sci. Emerg. Technol. 16 (2012) 211–217. https://doi.org/10.1016/j.ifset.2012.06.008.

[54] J.Y. Huang, Y.Y. Chieng, X. Li, W. Zhou, Experimental and Mathematical Assessment of Migration from Multilayer Food Packaging Containing a Novel Clay/Polymer Nanocomposite, Food Bioprocess Technol. 8 (2015) 382–393. https://doi.org/10.1007/s11947-014-1408-5.

[55] S. Maisanaba, R. Guzmán-Guillén, M. Puerto, D. Gutiérrez-Praena, N. Ortuño, Á. Jos, In vitro toxicity evaluation of new silane-modified clays and the migration extract from a derived polymer-clay nanocomposite intended to food packaging applications, J. Hazard. Mater. 341 (2018) 313–320. https://doi.org/10.1016/j.jhazmat.2017.08.003.

[56] A. Nasiri, E. Gastaldi, N. Gontard, S. Peyron, Multi-faceted migration in food contact polyethylene-based nanocomposite packaging, Appl. Clay Sci. 198 (2020) 105803. https://doi.org/10.1016/j.clay.2020.105803.

[57] Y. Echegoyen, S. Rodríguez, C. Nerín, Nanoclay migration from food packaging materials, Food Addit. Contam. - Part A Chem. Anal. Control. Expo. Risk Assess. 33 (2016) 530–539. https://doi.org/10.1080/19440049.2015.1136844.

[58] M. Farhoodi, S.M. Mousavi, R. Sotudeh-Gharebagh, Z. Emam-Djomeh, A. Oromiehie, Migration of aluminum and silicon from PET/clay nanocomposite bottles into acidic food simulant, Packag. Technol. Sci. 27 (2014) 161–168. https://doi.org/10.1002/pts.2017.

[59] Y. Echegoyen, C. Nerín, Nanoparticle release from nano-silver antimicrobial food containers, Food Chem. Toxicol. 62 (2013) 16–22. https://doi.org/10.1016/j.fct.2013.08.014.

[60] P. Vera, Y. Echegoyen, E. Canellas, C. Nerín, M. Palomo, Y. Madrid, C. Cámara, Nano selenium as antioxidant agent in a multilayer food packaging

material, Anal. Bioanal. Chem. 408 (2016) 6659–6670.

https://doi.org/10.1007/s00216-016-9780-9.

Supplementary information of

Exploring the boundaries in the analysis of large particles by single particle inductively coupled plasma mass spectrometry: Application to nanoclays

David Ojeda, Eduardo Bolea, Josefina Pérez-Arantegui, Francisco Laborda

Group of Analytical Spectroscopy and Sensors (GEAS)

Institute of Environmental Sciences (IUCA)

University of Zaragoza

Pedro Cerbuna 12, 50009 Zaragoza, Spain.

Index

S1. Isolation of particles below 1 µm from kaolin suspension by centrifugation

To isolate the fraction below 1 µm, the original product was suspended in ultrapure water at a starting concentration of 1000 mg L^{-1} of kaolin. After 1 hour of decantation, 15 mL of the supernatant were withdrawn from the suspension and finally centrifuged during 5 min at 1200 rpm. These conditions are the result of the calculations made considering the particles characterised were kaolinite ($Al_2Si_2O_5(OH_4)$), which is the main crystalline structure of the sample according to their analysis by X-ray diffraction, with a particle density of 2.6 g cm^{-3}. The mass fractions regarded for Al and Si are 18.0 and 21.7, respectively, determined from their molar fraction.

S2. Digestion of samples containing nanoclays for total Al analysis by ICP-MS

The procedure described by Inorganic Ventures for the elemental analysis of Zeolites was followed (https://www.inorganicventures.com/guides-and-papers/elemental-analysis-of-zeolites). It is based on the use of two reagents: UA-1 and UNS-1 (Inorganic Ventures, Christiansburg, USA). The first one is an acid reagent composed by HCl 20% (v/v) and HF 80% (v/v), whereas UNS-1 is a neutralising and a stabilising reagent which contains Triethylenetetramine (10-25% (v/v)). In this procedure the use of boric acid to eliminate the HF added in excess is unnecessary since pH conditions allow working with the fluorides mostly unprotonated. The procedure consists of the following steps, adapted to the sample conditions treated in this work:

1. A specific mass from the sample is weighed in a low density polyethylene bottle (LDPE) of 250 mL. Depending on the sample, the amount of mass is:

—For kaolin, 50 mg of original powder.

—For the fraction of particles below 1 μm of size from kaolin, 1 mL of suspension (supernatant after centrifugation).

—For the solutions from migration tests, either the material #1 or #2, 5 mL of volume.

2. In the case of solid samples, 10 drops of ultrapure water are added to the sample and then softly stirred, so the sample remains hydrated and not agglomerated.

3. 5 mL of reagent UA-1 and 0.25 mL o HNO_3 70% (v/v) J.T. Baker are added. The bottle is closed and it is shaken for over 2 minutes.

4. 25 mL of UNS-1 are added. The final weight is adjusted until 100 g with the addition of ultrapure water. The final solution is mixed by inverting it manually at least 50 times.

S3. Determination of limits of detection in terms of size and number concentration in SP-ICP-MS

Limits of detection (both in size and in number concentration) for the analysis by SP-ICP-MS in different conditions were calculated following the expressions:

$$LOD_{size} = X_C^{size} = \left(\frac{15\sigma_B}{\frac{1}{w_p}\pi\rho F_P K_{ICP-MS} K_M t_{dwell}} \right)^{1/3} \quad \text{(Eq. 2)}$$

$$LOD_{number} = \frac{5\sqrt{Y_{N,B}} + 3}{\eta Q_{sample} t_i} \quad \text{(Eq. 3)}$$

where σ_B is the standard deviation of the baseline of a blank, w_p the time-width for a transient particle event (in terms of time), ρ is the density, F_P is the mass fraction of the element in the particle, t_{dwell} is the dwell time, K_{ICP-MS} is the factor referred to the detection efficiency of the system, in which it is represented the ratio of the number of ions detected vs. the number of analyte atoms of the measured isotope into the ICP. K_M ($=AN_{Av}/M_M$)

is a factor related to the element measured, where A is the atomic abundance of the isotope considered, N_{Av} the Avogadro number, and M_M the atomic mass of the element. On the other hand, $Y_{N,B}$ is the number of events detected in the blank, η the transport efficiency, Q_{sample} is the sample introduction flow and t_i the acquisition time.

S4. Calculations for the determination of the upper size limit measurable by SP-ICP-MS

In the analysis of both SiO_2 and kaolinite particles (Sections 3.1 and 3.3, respectively) limitations related to the detector signal in pulse mode were observed for large particles. To estimate a limit above which the detector response would be affected, several profiles from the peaks detected by SP-ICP-MS during a measurement were studied. In the case of SiO_2 particles, using the isotope ^{29}Si, the maximum signal intensity was observed at 1560 counts (Figure S1a) for a dwell time of 100 µs.

Figure S1

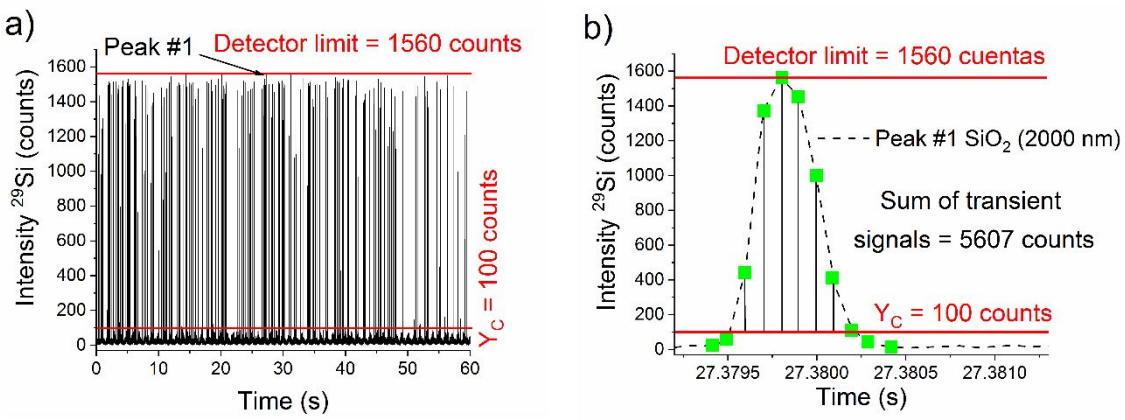

Figure S1. *a) Time scan for size standard of 2000 nm of SiO_2 particles for the study of the upper size limit, determined at 1560 counts. b) Profile of a single peak detected at the maximum intensity. Transient signals for the peak are displayed as green dots.*

Some peaks for the size standard of 2000 nm (nominal diameter) were confirmed to be uncompleted at this level, as can be seen in Figure S1b, whose profile is flattened at the top, losing some information in terms of intensity and, therefore, in terms of mass and size. Considering a width of 800 µs (the average value for the largest peaks detected with a complete profile), a symmetrical peak was modelled reaching the intensity of 1560 counts (Figure S2). Integrating its corresponding signal (sum of the transient signals) and transforming it into size, it was determined that the upper size limit (as equivalent diameter of a SiO_2 particle) was of 1200 nm, which means that below this size the characterisation would be correct under the conditions studied.

Figure S2

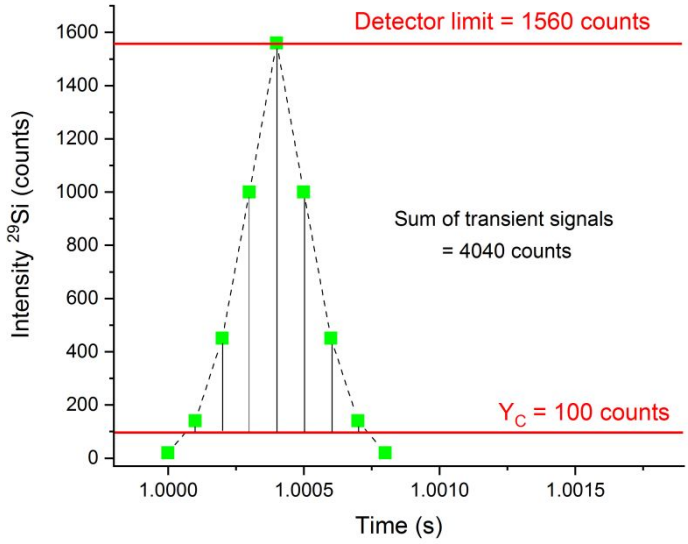

Figure S2. *Modelled peak for the size determination above which the characterisation of SiO_2 particles will be affected by limitations related to the detector, established in 1560 counts. Transient signals for the peak are displayed as green dots.*

For the kaolin, using the isotope ^{27}Al during the analysis, a maximum in the signal intensity was observed at 1625 counts (Figure S3). In a similar way, the modelled peak allowed to determine the upper size limit at 420 nm of equivalent diameter for kaolinite particles (Figure S4).

Figure S3

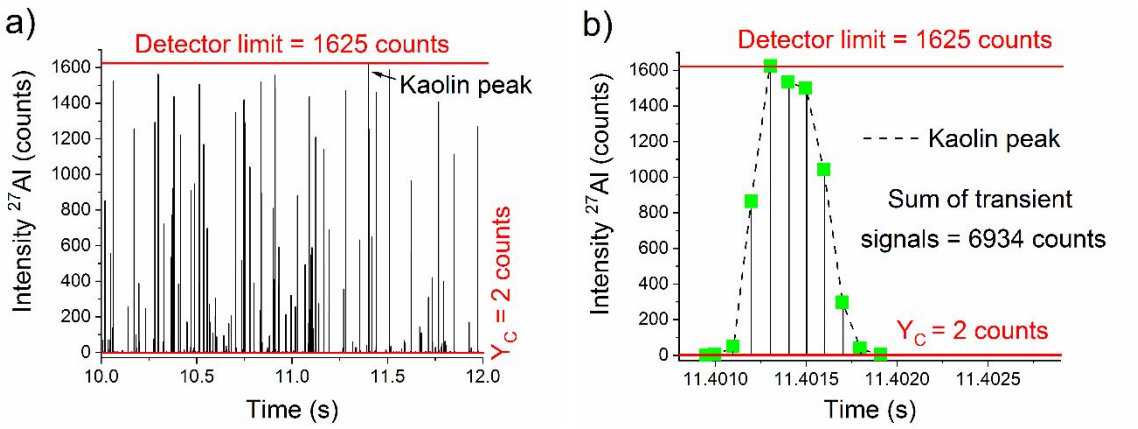

Figure S3. *a) Time scan for the fraction of particles below 1 µm from kaolin. b) Profile of a single peak detected at the maximum intensity for the study of the upper size limit, determined at 1625 counts. Transient signals for the peak are displayed as green dots.*

Figure S4

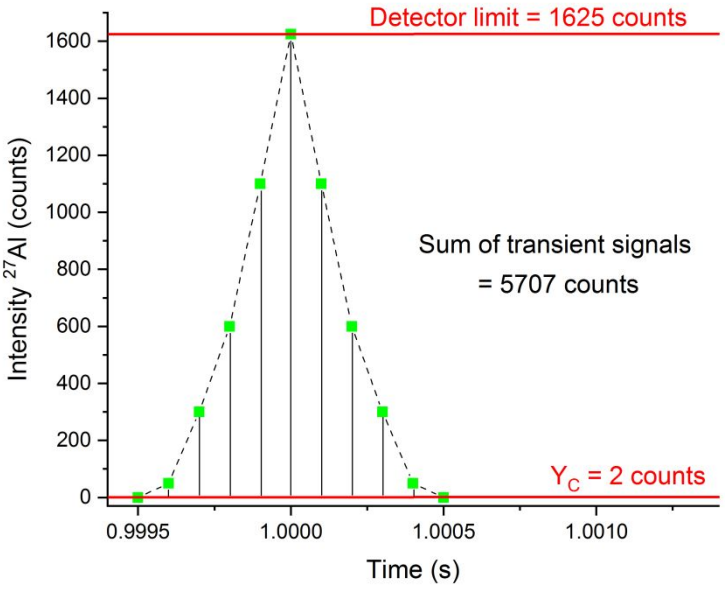

Figure S4. *Modelled peak for the size determination above which the characterisation of kaolinite particles will be affected by limitations related to the detector, established in 1625 counts. Transient signals for the peak are displayed as green dots.*

S5. Ionisation efficiency for SiO_2 particles

The mean intensity from peaks detected were plotted vs. the nominal size for different SiO_2 standards (500, 1000 and 2000 nm) to study their ionisation efficiencies (Figure S5). Given the linear relationship between the logarithms of these two parameters, a theoretical slope of 3 would be expected if ionisation of the particles were complete.

Figure S5

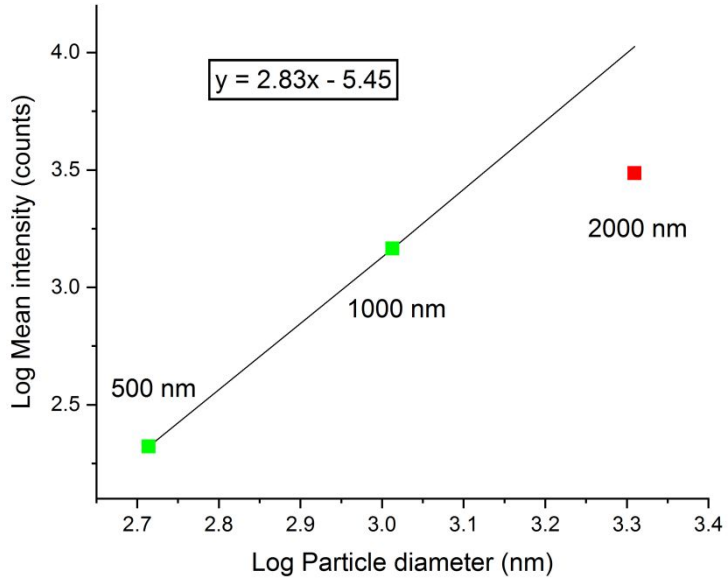

Figure S5. *Logarithm of the mean intensity obtained plotted vs. the logarithm of the nominal particle diameter for SiO_2 size standards of 500, 1000 and 2000 nm.*

S6. Analysis of Al_2O_3 particles by SP-ICP-MS using ^{27}Al

The method developed was applied to a commercial suspension of Al_2O_3 particles ranging from nominal size of 30 to 60 nm. Size distribution is shown in Figure S6, in accordance to the values specified by the manufacturer, and values of 40 nm as the most frequent size.

Figure S6

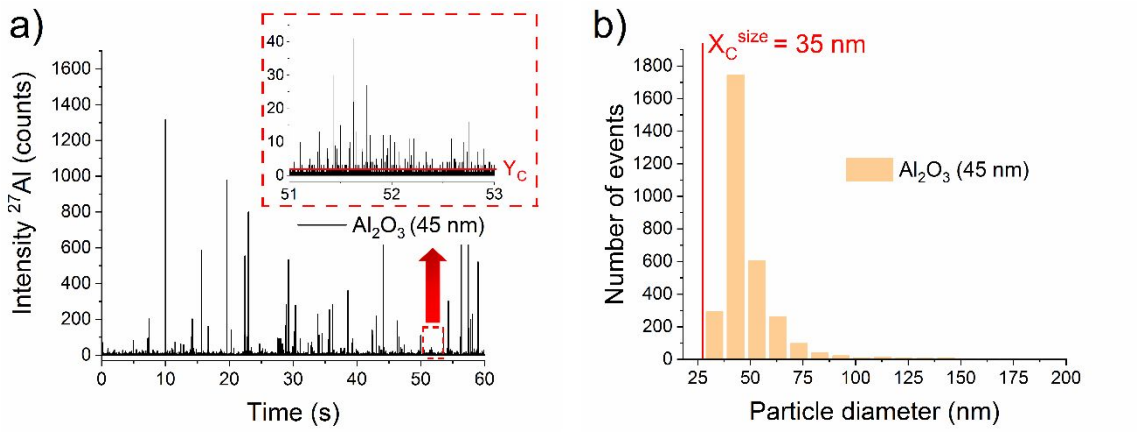

Figure S6. *Time scan using ^{27}Al for Al_2O_3 particles from a commercial suspension (45 nm of nominal size). b) Particle size distribution obtained by SP-ICP-MS. Critical value (Y_C) applied of 2 counts, which in terms of size equals 35 nm (X_C^{size}).*

The use of ^{27}Al as the isotope of analysis allowed to reduce the LOD_{size} to 35 nm in comparison to ^{29}Si. Given the proximity to the critical value (Y_C), the distribution obtained is not complete, with a nebulization efficiency of 35%, as can be seen in Table S1.

Table S1. *Size characterisation of Al_2O_3 particles from a commercial suspension by SP-ICP-MS. Most frequent size shown in brackets. Results for ^{27}Al, expressed as mean ± s (n = 3).*

Al_2O_3 suspension*	**Average peak intensity (counts)**	**Average diameter (nm)**	**Nº of events**	**Nebulisation efficiency (%)**
45 nm (30 - 60 nm)	21 ± 2	50 ± 1 (43 ± 2)	3128 ± 36	34.9 ± 0.4

* Average nominal diameter and distribution (in brackets) specified by the manufacturer, determined by TEM.

S7. Determination of thickness for kaolinite particles in TEM images

Average values of thickness were determined by EELS for the calculation of equivalent diameters of kaolinite particles shown in TEM images (Figure S7).

Figure S7

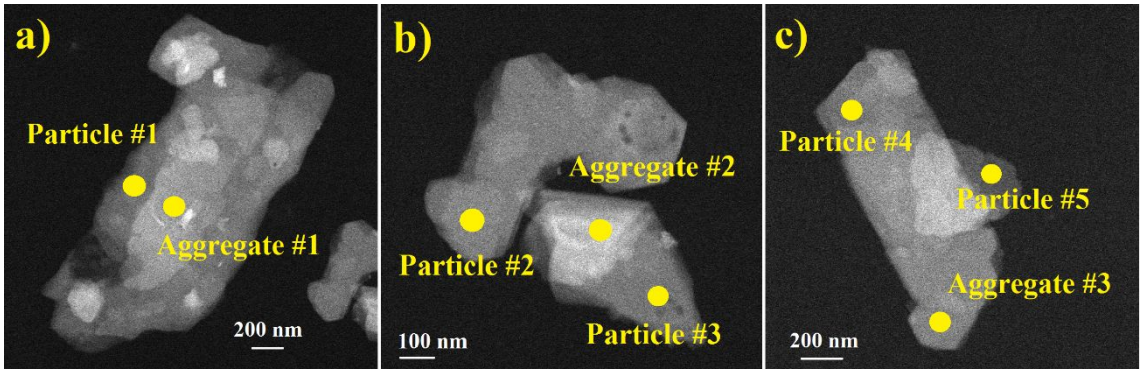

Figure S7. *HAADF-TEM images of kaolinite particles (fraction below 1 μm) for the thickness determination by EELS, differentiating between individual laminates and aggregates.*

Two different methods were compared: log-ratio absolute and Kramers-Kronig sum, obtaining similar results in both cases (verified by *t-test*, 95% confidence interval). Given the aggregation of particles observed by TEM, two different average thicknesses were determined: 50 nm for individual particles and 80 nm for aggregates (Table S2).

Table S2. *Thickness determination for kaolinite particles by EELS with two different methods. Results shown as the average ± s (n = 5).*

Kaolinite particles	**Average thickness from two methods (nm)**	
	Log-ratio absolute	**Kramers-Kronig**
Individual particles	56.2 ± 6.2	53.3 ± 2.9
Aggregates	78.6 ± 4.3	73.2 ± 6.1

S8. Migrated particles from material #1 observed by TEM

Particles of several micrometers were observed by TEM (Figure S8a) with high contents in carbon. Inside these particles, hexagonal structures with presence of aluminium and silicon were confirmed by EDS spectra (Figure S8b).

Figure S8

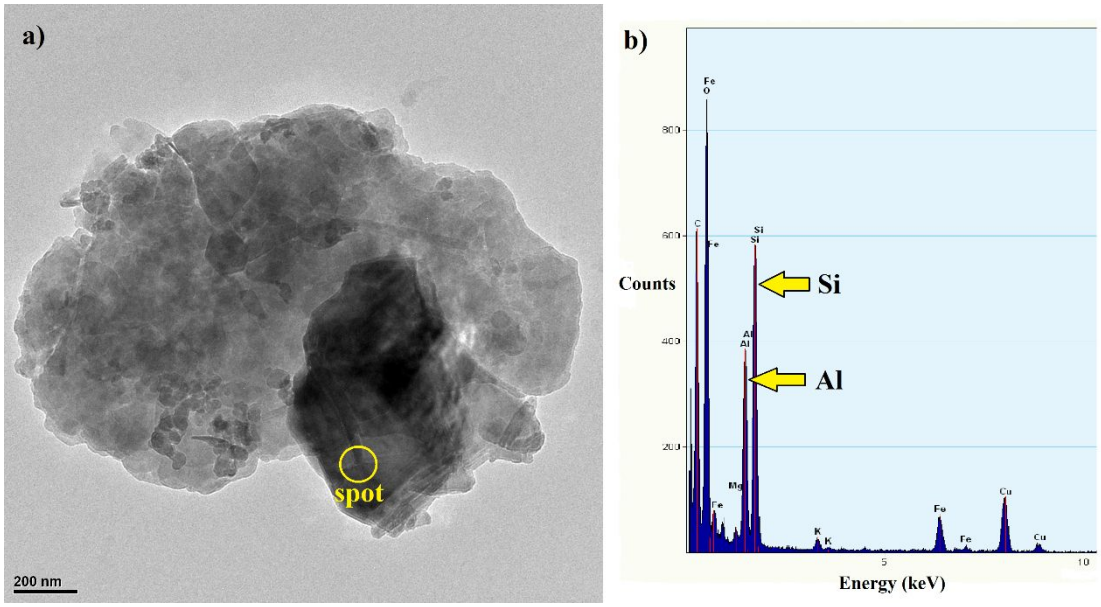

Figure S8. *a) TEM image of a microfragment migrated from material #1, with hexagonal structures embedded containing Al and Si. b) EDS spectre for the spot highlighted.*